SAND2019-2747C

Initial Potential-Based Time Domain Surface Integral Equations for Dielectric Regions

T. E. Roth[1,2] and W. C. Chew[2,3]

[1]Sandia National Laboratories, Albuquerque, New Mexico, USA
[2]Department of Electrical and Computer Engineering, University of Illinois at Urbana-Champaign, Urbana, Illinois, USA
[3]School of Electrical and Computer Engineering, Purdue University, West Lafayette, Indiana, USA

Abstract— The **A**-Φ formulation has been proposed as a new paradigm for deriving computational electromagnetics methods with no low frequency breakdown, and that are more directly applicable to coupling into quantum physics problems of interest. This formulation utilizes equations developed in terms of the magnetic vector potential (**A**) and electric scalar potential (Φ), which are deemed more fundamental quantities for quantum applications than the electric and magnetic fields. Further, computational electromagnetics solvers developed from the **A**-Φ formulation have been successful at overcoming many of the inherent multiscale limitations that exist for field-based solvers. This has been shown in recent work, where time domain integral equations (TDIEs) applicable to perfect electric conductor (PEC) objects were shown to be stable and accurate over broad frequency ranges. However, many quantum electromagnetics applications of interest are pursued at optical frequencies where approximating metals as PEC is no longer acceptable. Instead, these regions are more appropriately described with a Drude-Lorentz-Sommerfeld model; and so computational electromagnetics solvers applicable to multiscale geometries that can analyze these regions over very broad frequency ranges are needed. This current work begins to address this need by presenting for the first time in either frequency or time domain a set of **A**-Φ formulation surface integral equations applicable to simple, loss-free dielectric regions. To do this, we derive TDIEs based on recently developed integral representation of solutions to the wave equations for **A** and Φ. A rigorous functional framework that was used to analyze the stability of the PEC **A**-Φ formulation TDIEs is leveraged to determine appropriate combinations of integral equations and unknowns so that stable marching-on-in-time discretization approaches for the dielectric TDIEs can be developed here. The result is a set of **A**-Φ formulation TDIEs with appropriate discretization guidelines that can accurately and stably analyze dielectric regions at middle frequencies. Although not applicable at very low frequencies, these equations provide an essential step toward this goal by determining a baseline for combinations of equations and unknowns for dielectric regions within this formulation.

1. INTRODUCTION

Modern applications of electromagnetic and quantum physics require computational electromagnetics (CEM) tools to analyze traditionally challenging problems; namely, the very broadband analysis of multiscale/subwavelength dielectric geometries [1, 2, 3, 4]. This is largely driven by many applications operating at near-optical wavelengths, where approximations of metals as perfect conductors no longer apply [1]. These challenging problems necessitate new CEM methods, such as the **A**-Φ formulation, which attempts to address these needs by formulating CEM methods directly in terms of the magnetic vector (**A**) and electric scalar (Φ) potentials [5, 6]. However, these potential-based integral equation formulations to date have only been applicable to perfectly conducting objects; making them inapplicable to many quantum applications of interest.

This work begins to address this by presenting a set of potential-based time domain integral equations (TDIEs) for dielectric regions based on frequency domain integral representation formulas derived in [5]. Further, we provide guidelines based on rigorous functional analysis of similar integral equations for what basis and testing functions can be used in a marching-on-in-time (MOT) discretization to achieve stable results in practice [7, 8]. In lieu of this analysis for these equations, we demonstrate the stability and accuracy of this formulation at middle frequencies through numerical results.

The remainder of this work is organized into the following sections. Section 2 presents the derivation of the potential-based TDIEs applicable to dielectric regions. Following this, Section 3 provides details on MOT discretizations of these equations to achieve stable results. Section 4 then demonstrates the qualities of these new TDIEs through appropriate numerical examples. Finally, Section 5 discusses conclusions and future work related to potential-based TDIEs.

Sandia National Laboratories is a multimission laboratory managed and operated by National Technology & Engineering Solutions of Sandia, LLC, a wholly owned subsidiary of Honeywell International Inc., for the U.S. Department of Energy's National Nuclear Security Administration under contract DE-NA0003525.

2. FORMULATION

Before integral representation formulas for the different potentials may be discussed, it is necessary to determine the partial differential equations (PDEs) that the potentials should obey. A standard approach to this introduces the potentials so that Maxwell's equations are automatically satisfied [5]. In particular, by letting

$$\mathbf{B} = \nabla \times \mathbf{A}, \tag{1}$$

$$\mathbf{E} = -\dot{\mathbf{A}} - \nabla\Phi, \tag{2}$$

and utilizing the Lorenz gauge,

$$\nabla \cdot \mathbf{A} = -\mu\epsilon\dot{\Phi}, \tag{3}$$

it can be easily seen that $\mathbf{A}$ and Φ must satisfy the following two wave equations:

$$\nabla^2\mathbf{A} - \mu\epsilon\ddot{\mathbf{A}} = -\mu\mathbf{J} \tag{4}$$

$$\nabla^2\Phi - \mu\epsilon\ddot{\Phi} = -\rho/\epsilon. \tag{5}$$

To simplify the derivation of integral representation formulas, we will perform it in the frequency domain and then transform the results to the time domain. Assuming an $\exp(-i\omega t)$ time dependence, the wave equations for the potentials in the frequency domain are

$$\nabla^2\mathbf{A} + k^2\mathbf{A} = -\mu\mathbf{J} \tag{6}$$

$$\nabla^2\Phi + k^2\Phi = -\rho/\epsilon, \tag{7}$$

where $k^2 = \omega^2\mu\epsilon$. With the relevant wave equations determined, the integral representation formulas for the two potentials may be derived.

2.1. Integral Representation Formulas

2.1.1. Frequency Domain

For simplicity, the representation formula for Φ will be derived first. To begin, consider any closed, homogeneous domain Ω_i with boundary S, and its companion space $\Omega_e = \mathbb{R}^3 \setminus \Omega_i$. Then an integral representation for Φ can be found, where Φ is a solution of the wave equation in $\mathbb{R}^3 \setminus S$, equal to Φ_e in Ω_e and Φ_i in Ω_i.

In the absence of sources, the potential in Ω_i must satisfy

$$(\nabla^2 + k^2)\Phi_i(\mathbf{r}) = 0. \tag{8}$$

Similarly, a Green's function may be defined within Ω_i that must satisfy

$$(\nabla^2 + k^2)g(\mathbf{r}, \mathbf{r}') = -\delta(\mathbf{r} - \mathbf{r}'). \tag{9}$$

The classic example of a function satisfying this equation and the radiation condition is the homogeneous medium Green's function, i.e.,

$$g(\mathbf{r}, \mathbf{r}') = \frac{e^{ikR}}{4\pi R}. \tag{10}$$

Now, multiplying (8) by $g(\mathbf{r}, \mathbf{r}')$ and (9) by Φ and subtracting the resulting equations gives

$$\int_{\Omega_i} \Big(g(\mathbf{r}, \mathbf{r}')\nabla^2\Phi_i(\mathbf{r}) - \Phi_i(\mathbf{r})\nabla^2 g(\mathbf{r}, \mathbf{r}' \Big) d\Omega_i = \Phi(\mathbf{r}'), \quad \mathrm{r}' \in \Omega_i. \tag{11}$$

Applying the divergence theorem and then swapping the role of $\mathbf{r}$ and $\mathbf{r}'$ we arrive at the following surface integral,

$$\int_S \Big(g(\mathbf{r}, \mathbf{r}')\hat{n}' \cdot \nabla'\Phi_i(\mathbf{r}') - \hat{n}' \cdot \nabla' g(\mathbf{r}, \mathbf{r}')\Phi_i(\mathbf{r}') \Big) dS' = \Phi_i(\mathbf{r}), \quad \mathrm{r} \notin S,\, \mathrm{r} \in \Omega_i, \tag{12}$$

where $\hat{n}'$ is the outward pointing normal to S at $\mathbf{r}'$. A similar process can be performed in the exterior domain Ω_e. Adding the contributions from the two regions together gives

$$\int_S \Big(g(\mathbf{r},\mathbf{r}')p(\mathbf{r}') - \hat{n}'\cdot\nabla' g(\mathbf{r},\mathbf{r}')\varphi(\mathbf{r}') \Big) dS' = \Phi(\mathbf{r}), \quad \mathrm{r} \notin S, \tag{13}$$

where $\varphi = \Phi_i - \Phi_e$ and $p = \hat{n}'\cdot\nabla'\Phi_i - \hat{n}'\cdot\nabla'\Phi_e$ are the jumps of Φ and its normal derivative across S. This integral representation of Φ is essential for deriving surface integral equations that solve the scalar wave equation [7, 9].

At this point, the integral representation formula can be seen as simply producing solutions to the wave equation given in (7). So that the potential actually represents an electromagnetic potential (i.e., it solves Maxwell's equations), it is essential that the Lorenz gauge be applied to "tie" the potentials together correctly [10]. This can be done by utilizing the current continuity equation when the charge density is written in terms of the potentials. In particular, for the surface current densities that are of interest to solving integral equations, the current continuity equation becomes

$$\frac{\nabla'\cdot\mathbf{J}}{i\omega\epsilon} = -(\Pi + p), \tag{14}$$

where $\Pi = -i\omega\hat{n}'\cdot(\mathbf{A}_i - \mathbf{A}_e)$, and $\nabla\cdot\mathbf{J}$ should also be thought of as being defined by "jumps" in the value on either side of S. Considering this, (13) becomes

$$\int_S \Big(\frac{i}{\omega\epsilon} g(\mathbf{r},\mathbf{r}')\nabla'\cdot\mathbf{J}(\mathbf{r}') - g(\mathbf{r},\mathbf{r}')\Pi(\mathbf{r}') + \hat{n}'\cdot\nabla' g(\mathbf{r},\mathbf{r}')\frac{1}{i\omega}\Psi(\mathbf{r}') \Big) dS' = \Phi(\mathbf{r}), \quad \mathrm{r} \notin S, \tag{15}$$

where $\Psi = -i\omega\varphi$. This change is made so that Ψ has the same temporal regularity as the other surface sources (e.g. Π), and so, will be able to be discretized using the same temporal basis functions [7].

With the basic process understood, it is now necessary to derive a similar integral representation formula for $\mathbf{A}$. Considering the similarity of the vector and scalar potential wave equations, it can be immediately seen that a possible integral representation for $\mathbf{A}$ is [5]

$$\int_S \Big(g(\mathbf{r},\mathbf{r}')\hat{n}'\cdot\nabla'\mathbf{A}(\mathbf{r}') - \hat{n}'\cdot\nabla' g(\mathbf{r},\mathbf{r}')\mathbf{A}(\mathbf{r}') \Big) dS' = \mathbf{A}(\mathbf{r}), \quad \mathrm{r} \notin S. \tag{16}$$

Although formally correct, this integral representation is of limited use in practical applications. Instead, an equivalent form that is more useful and can be derived using a generalized Green's theorem, as shown in detail in [5], is

$$\begin{aligned} -\int_S \Big(& g(\mathbf{r},\mathbf{r}')\big[\hat{n}'\times\nabla'\times\mathbf{A}(\mathbf{r}')\big] - \nabla' g(\mathbf{r},\mathbf{r}')\times\big[\hat{n}'\times\mathbf{A}(\mathbf{r}')\big] \\ & - \hat{n}' g(\mathbf{r},\mathbf{r}')\nabla'\cdot\mathbf{A}(\mathbf{r}') + \nabla' g(\mathbf{r},\mathbf{r}')\hat{n}'\cdot\mathbf{A}(\mathbf{r}') \Big) dS' = \mathbf{A}(\mathbf{r}), \quad \mathbf{r} \notin S. \end{aligned} \tag{17}$$

Similar to the scalar potential integral representation, it is essential that the Lorenz gauge be applied to "tie" the potentials together in (17). Performing this gives an updated integral representation suitable for electromagnetic problems as

$$\begin{aligned} -\int_S \Big(& \mu g(\mathbf{r},\mathbf{r}')\mathbf{J}(\mathbf{r}') + \nabla' g(\mathbf{r},\mathbf{r}')\times\frac{1}{i\omega}\mathbf{m}(\mathbf{r}') + \hat{n}' g(\mathbf{r},\mathbf{r}')\mu\epsilon\Psi(\mathbf{r}') \\ & - \frac{1}{i\omega}\nabla' g(\mathbf{r},\mathbf{r}')\Pi(\mathbf{r}') \Big) dS' = \mathbf{A}(\mathbf{r}), \quad \mathbf{r} \notin S, \end{aligned} \tag{18}$$

where $\mu\mathbf{J} = \big[\hat{n}'\times\nabla'\times\mathbf{A}\big]$ and $\mathbf{m} = -i\omega\hat{n}'\times\mathbf{A}$ has been used. Note again that surface sources are selected so they have the same temporal regularity as each other. Utilizing the integral representations given in (15) and (18), surface integral equations that perform well from very low to high frequencies for PEC objects have been derived [5, 6, 11]. As will be shown shortly, these integral representations may also be used to derive integral equations applicable to solving problems involving penetrable media (e.g., dielectric objects).

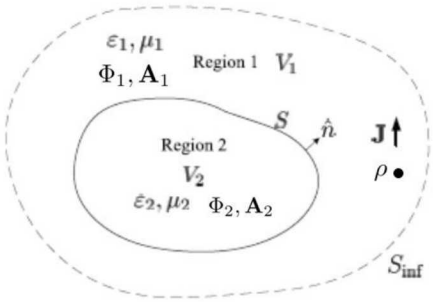

Figure 1: Configuration of a two region problem.

2.1.2. Time Domain

Time domain integral representations of the potentials can be derived by taking inverse Fourier transforms of the frequency domain formulas. Although performing this is quite simple, it is important that care be taken in the overall derivation to arrive at TDIEs that may be stably discretized with the MOT method.

Starting with the scalar potential representation given in (15), the time domain version is

$$\int_S \left(\int_{-\infty}^{\tau} \frac{\nabla \cdot \mathbf{J}(\mathbf{r}', t')}{4\pi R \epsilon} dt' - \frac{\Pi(\mathbf{r}', \tau)}{4\pi R} - \hat{n}' \cdot \nabla' \int_{-\infty}^{\tau} \frac{\Psi(\mathbf{r}', t')}{4\pi R} dt' \right) dS' = \Phi(\mathbf{r}), \quad \mathrm{r} \notin S, \tag{19}$$

where $\tau = t - R/c$ is the retarded time and c is the speed of light. Similarly, the integral representation for $\mathbf{A}$ given in (18) becomes

$$-\int_S \left(\mu \frac{\mathbf{J}(\mathbf{r}', \tau)}{4\pi R} - \nabla \int_{-\infty}^{\tau} \frac{\Pi(\mathbf{r}', t')}{4\pi R} dt' + \hat{n}' \mu \epsilon \frac{\Psi(\mathbf{r}', \tau)}{4\pi R} + \nabla \times \int_{-\infty}^{\tau} \frac{\mathbf{m}(\mathbf{r}', t')}{4\pi R} \right) dS' = \mathbf{A}(\mathbf{r}), \quad \mathbf{r} \notin S. \tag{20}$$

2.2. Surface Integral Equations

A number of approaches exist to derive integral equations to solve electromagnetics problems composed of piecewise homogeneous regions. One standard way is to independently formulate an equation for the field/potential in each region in terms of surface unknowns and to then tie the solutions in each region together using boundary conditions [9]. This process will be performed for the scenario shown in Fig. 1 using the integral representations derived in the previous sections.

To begin, we note some relevant boundary conditions that need to be satisfied on S. These are

$$\begin{cases} \hat{n} \times \mathbf{A}_1 = \hat{n} \times \mathbf{A}_2 \\ \hat{n} \cdot \epsilon_1 \mathbf{A}_1 = \hat{n} \cdot \epsilon_2 \mathbf{A}_2 \\ \Phi_1 = \Phi_2 \\ \hat{n} \times \mathbf{H}_1 = \hat{n} \times \mathbf{H}_2 \end{cases} \tag{21}$$

where the subscripts denote the region that the *total* (i.e., incident and scattered) potential or field are defined in [5]. Our goal is to derive integral equations for each region independently that can be tied together using (21) and produce the correct potentials in each region.

2.2.1. Exterior Integral Equations

With this in mind, we first formulate an integral equation for the exterior region (region 1 in Fig. 1). This is done by associating with the actual PDE to be solved in the exterior region another auxiliary PDE in the interior region. We have the freedom to choose the interior PDE in an advantageous

way, as will be seen shortly. The exterior PDE that needs to be solved is

$$\begin{cases} \nabla^2\Phi_1(\mathbf{r},t) - \mu_1\epsilon_1\ddot{\Phi}_1(\mathbf{r},t) = -\rho/\epsilon_1 \quad \text{in } V_1 \times \mathbb{R}_+ \\ \nabla^2\mathbf{A}_1(\mathbf{r},t) - \mu_1\epsilon_1\ddot{\mathbf{A}}_1(\mathbf{r},t) = -\mu_1\mathbf{J} \quad \text{in } V_1 \times \mathbb{R}_+ \\ \Phi_1(\mathbf{r},0), \dot{\Phi}_1(\mathbf{r},0) = 0 \quad \text{in } V_1 \\ \mathbf{A}_1(\mathbf{r},0), \dot{\mathbf{A}}_1(\mathbf{r},0) = 0 \quad \text{in } V_1 \\ \Phi_1(\mathbf{r},t) = \Phi_2(\mathbf{r},t) \quad \text{on } S \times \mathbb{R}_+ \\ \hat{n} \times \big[\mathbf{A}_1(\mathbf{r},t) \times \hat{n}\big] = \hat{n} \times \big[\mathbf{A}_2(\mathbf{r},t) \times \hat{n}\big] \quad \text{on } S \times \mathbb{R}_+. \end{cases} \tag{22}$$

As previously mentioned, we need to associate with this external problem an auxiliary internal problem that will allow us to solve the entire problem. This will require having the different "jumps" in the surface sources across S be equal to the total potentials or fields in region 1. This can be done by choosing surface sources so that the scattered potential in region 2 (denoted as Φ_i) cancels the incident potential at all times (e.g., $\Phi_i = -\Phi_{\text{inc}}$), producing the well-known extinction theorem [5, 9].

Using the results in Section 2.1, we now have the following integral representation for the scattered potential in region 1 (denoted as Φ_e):

$$\begin{cases} \mathbf{r} \in V_1, & \Phi_e \\ \mathbf{r} \in V_2, & -\Phi_{\text{inc}} \end{cases} = -\int_S \bigg(\int_{-\infty}^{\tau_1} \frac{\nabla \cdot \mathbf{J}_1(\mathbf{r}',t')}{4\pi R\epsilon_1} dt' - \frac{\Pi_1(\mathbf{r}',\tau_1)}{4\pi R} - \hat{n}' \cdot \nabla' \int_{-\infty}^{\tau_1} \frac{\Psi_1(\mathbf{r}',t')}{4\pi R} dt' \bigg) dS', \tag{23}$$

where $\tau_1 = t - R/c_1$. To arrive at a surface integral equation, we note that by continuity of the total scalar potential we have

$$\Phi_1 = \Phi_e + \Phi_{\text{inc}} = \Phi_i + \Phi_{\text{inc}} = 0, \quad \mathbf{r} \in S. \tag{24}$$

Plugging in our representation for Φ_e and taking the limit as $\mathbf{r}$ approaches S (from V_1) we arrive at the following integral equation:

$$\begin{aligned} \int_S \bigg(-\int_{-\infty}^{\tau_1} \frac{\nabla \cdot \mathbf{J}_1(\mathbf{r}',t')}{4\pi R\epsilon_1} dt' + \frac{\Pi_1(\mathbf{r}',\tau_1)}{4\pi R} \bigg) dS' + \frac{1}{2}\int_{-\infty}^{t} \Psi_1(\mathbf{r},t')dt' \\ + \int_S \hat{n}' \cdot \hat{R} \bigg(\int_{-\infty}^{\tau_1} \frac{\Psi_1(\mathbf{r}',t')}{4\pi R^2} dt' + \frac{\Psi_1(\mathbf{r}',\tau_1)}{4\pi R c_1} \bigg) dS' = -\Phi_{\text{inc}}, \quad \mathbf{r} \in S. \end{aligned} \tag{25}$$

Following similar steps, but for the vector potential, we have

$$\begin{aligned} \int_S \bigg(\mu_1 \frac{\mathbf{J}_1(\mathbf{r}',\tau_1)}{4\pi R} - \nabla \int_{-\infty}^{\tau_1} \frac{\Pi_1(\mathbf{r}',t')}{4\pi R} dt' + \hat{n}'\mu_1\epsilon_1 \frac{\Psi_1(\mathbf{r}',\tau_1)}{4\pi R} \bigg) dS' + \frac{1}{2}\int_{-\infty}^{t} \hat{n}' \times \mathbf{m}_1(\mathbf{r},t')dt' \\ - \int_S \hat{R} \times \bigg[\int_{-\infty}^{\tau_1} \frac{\mathbf{m}_1(\mathbf{r}',t')}{4\pi R^2} dt' + \frac{\mathbf{m}_1(\mathbf{r}',\tau_1)}{4\pi R c_1} \bigg] dS' = -\hat{n} \times \big[\mathbf{A}_{\text{inc}}(\mathbf{r}) \times \hat{n}\big], \quad \mathbf{r} \in S. \end{aligned} \tag{26}$$

At this point, we have derived two coupled integral equations for four unknown functions. To arrive at a solvable system, we will need two more integral equations. These can be derived by considering integral equations derived in the internal region.

2.2.2. Interior Integral Equations

A similar process can be taken for deriving integral equations in the interior domain. However, because there are no incident potentials (for the scenario shown in Fig. 1) the PDEs are slightly different. In particular, we start with the interior region, V_2, with the following PDE:

$$\begin{cases} \nabla^2\Phi_2(\mathbf{r},t) - \mu_2\epsilon_2\ddot{\Phi}_2(\mathbf{r},t) = 0 \quad \text{in } V_2 \times \mathbb{R}_+ \\ \nabla^2\mathbf{A}_2(\mathbf{r},t) - \mu_2\epsilon_2\ddot{\mathbf{A}}_2(\mathbf{r},t) = 0 \quad \text{in } V_2 \times \mathbb{R}_+ \\ \Phi_2(\mathbf{r},0), \dot{\Phi}_2(\mathbf{r},0) = 0 \quad \text{in } V_2 \\ \mathbf{A}_2(\mathbf{r},0), \dot{\mathbf{A}}_2(\mathbf{r},0) = 0 \quad \text{in } V_2 \\ \Phi_2(\mathbf{r},t) = \Phi_1(\mathbf{r},t) \quad \text{on } S \times \mathbb{R}_+ \\ \hat{n} \times \big[\mathbf{A}_2(\mathbf{r},t) \times \hat{n}\big] = \hat{n} \times \big[\mathbf{A}_1(\mathbf{r},t) \times \hat{n}\big] \quad \text{on } S \times \mathbb{R}_+. \end{cases} \tag{27}$$

Given there are no incident potentials we formulate the exterior PDE with a solution of null potentials.

From this, we have as an integral representation of the solution the following:

$$\begin{cases} \mathbf{r} \in V_1, & 0 \\ \mathbf{r} \in V_2, & \Phi_2 \end{cases} = \int_S \left(\int_{-\infty}^{\tau_2} \frac{\nabla \cdot \mathbf{J}_2(\mathbf{r}', t')}{4\pi R \epsilon_2} dt' - \frac{\Pi_2(\mathbf{r}', \tau_2)}{4\pi R} - \hat{n}' \cdot \nabla' \int_{-\infty}^{\tau_2} \frac{\Psi_2(\mathbf{r}', t')}{4\pi R} dt' \right) dS', \quad (28)$$

where $\tau_2 = t - R/c_2$. From the continuity of the scalar potential on S we have that

$$\Phi_2 = 0, \quad \mathbf{r} \in S. \quad (29)$$

Plugging in our representation for Φ_2 and taking the limit as $\mathbf{r}$ approaches S (from V_2) we arrive at the following integral equation:

$$\int_S \left(- \int_{-\infty}^{\tau_2} \frac{\nabla \cdot \mathbf{J}_2(\mathbf{r}', t')}{4\pi R \epsilon_2} dt' + \frac{\Pi_2(\mathbf{r}', \tau_2)}{4\pi R} \right) dS' - \frac{1}{2} \int_{-\infty}^{t} \Psi_2(\mathbf{r}, t') dt' + \int_S \hat{n}' \cdot \hat{R} \left(\int_{-\infty}^{\tau_2} \frac{\Psi_2(\mathbf{r}', t')}{4\pi R^2} dt' + \frac{\Psi_2(\mathbf{r}', \tau_2)}{4\pi R c_2} \right) dS' = 0, \quad \mathbf{r} \in S. \quad (30)$$

Similarly for the vector potential, we have

$$\int_S \left(\mu_2 \frac{\mathbf{J}_2(\mathbf{r}', \tau_2)}{4\pi R} - \nabla \int_{-\infty}^{\tau_2} \frac{\Pi_2(\mathbf{r}', t')}{4\pi R} dt' + \hat{n}' \mu_2 \epsilon_2 \frac{\Psi_2(\mathbf{r}', \tau_2)}{4\pi R} \right) dS' - \frac{1}{2} \int_{-\infty}^{t} \hat{n}' \times \mathbf{m}_2(\mathbf{r}, t') dt' - \int_S \hat{R} \times \left[\int_{-\infty}^{\tau_2} \frac{\mathbf{m}_2(\mathbf{r}', t')}{4\pi R^2} dt' + \frac{\mathbf{m}_2(\mathbf{r}', \tau_2)}{4\pi R c_2} \right] dS' = 0, \quad \mathbf{r} \in S. \quad (31)$$

We have now derived four integral equations in total. However, it is clear that the unknown functions are different between (25)-(26) and (30)-(31). This can be resolved by utilizing the overall boundary conditions for the problem, given in (21).

2.2.3. Complete Integral Equation System

Considering the boundary conditions in (21), we see that in all but one case the equivalent sources defined in the exterior and interior integral equations are the same. The one equivalent source that needs to be adjusted is $\Pi = \hat{n} \cdot \dot{\mathbf{A}}$, which can be simply done by noting that

$$\Pi_2 = \frac{\epsilon_1}{\epsilon_2} \Pi_1. \quad (32)$$

Performing this replacement and removing the now redundant subscripts on the unknowns, we arrive at the final surface integral equation system to be solved. This is:

$$\int_S \left(\mu_1 \frac{\mathbf{J}(\mathbf{r}', \tau_1)}{4\pi R} - \nabla \int_{-\infty}^{\tau_1} \frac{\Pi(\mathbf{r}', t')}{4\pi R} dt' + \hat{n}' \mu_1 \epsilon_1 \frac{\Psi(\mathbf{r}', \tau_1)}{4\pi R} \right) dS' + \frac{1}{2} \int_{-\infty}^{t} \hat{n}' \times \mathbf{m}(\mathbf{r}, t') dt' - \int_S \hat{R} \times \left[\int_{-\infty}^{\tau_1} \frac{\mathbf{m}(\mathbf{r}', t')}{4\pi R^2} dt' + \frac{\mathbf{m}(\mathbf{r}', \tau_1)}{4\pi R c_1} \right] dS' = -\hat{n} \times \left[\mathbf{A}_{\text{inc}}(\mathbf{r}) \times \hat{n} \right], \quad \mathbf{r} \in S, \quad (33)$$

$$\int_S \left(- \int_{-\infty}^{\tau_1} \frac{\nabla \cdot \mathbf{J}(\mathbf{r}', t')}{4\pi R \epsilon_1} dt' + \frac{\Pi(\mathbf{r}', \tau_1)}{4\pi R} \right) dS' + \frac{1}{2} \int_{-\infty}^{t} \Psi(\mathbf{r}, t') dt' + \int_S \hat{n}' \cdot \hat{R} \left(\int_{-\infty}^{\tau_1} \frac{\Psi(\mathbf{r}', t')}{4\pi R^2} dt' + \frac{\Psi(\mathbf{r}', \tau_1)}{4\pi R c_1} \right) dS' = -\Phi_{\text{inc}}, \quad \mathbf{r} \in S, \quad (34)$$

$$\int_S \left(\mu_2 \frac{\mathbf{J}(\mathbf{r}', \tau_2)}{4\pi R} - \nabla \int_{-\infty}^{\tau_2} \frac{\Pi(\mathbf{r}', t')}{4\pi R} dt' + \hat{n}' \mu_2 \epsilon_2 \frac{\Psi(\mathbf{r}', \tau_2)}{4\pi R} \right) dS' + \frac{1}{2} \int_{-\infty}^{t} \hat{n}' \times \mathbf{m}(\mathbf{r}, t') dt' - \int_S \hat{R} \times \left[\int_{-\infty}^{\tau_2} \frac{\mathbf{m}(\mathbf{r}', t')}{4\pi R^2} dt' + \frac{\mathbf{m}(\mathbf{r}', \tau_2)}{4\pi R c_2} \right] dS' = 0, \quad \mathbf{r} \in S, \quad (35)$$

$$\int_S \Bigg(-\int_{-\infty}^{\tau_2} \frac{\nabla\cdot\mathbf{J}(\mathbf{r}',t')}{4\pi R\epsilon_2}dt' + \frac{\epsilon_1}{\epsilon_2}\frac{\Pi(\mathbf{r}',\tau_2)}{4\pi R}\Bigg)dS' + \frac{1}{2}\int_{-\infty}^{t}\Psi(\mathbf{r},t')dt' + \int_S \hat{n}'\cdot\hat{R}\Bigg(\int_{-\infty}^{\tau_2}\frac{\Psi(\mathbf{r}',t')}{4\pi R^2}dt' + \frac{\Psi(\mathbf{r}',\tau_2)}{4\pi Rc_2}\Bigg)dS' = 0, \quad \mathbf{r}\in S. \quad (36)$$

3. DISCRETIZATION

With the necessary integral equations now derived, the discretization can be discussed. As was pointed out previously, the time domain discretization of these potential-based integral equations is complicated by the need to determine correct basis and testing functions to ensure stability of the overall method. To do this, rigorous functional analysis of the integral equations within appropriate Sobolev spaces are necessary [7]. This type of analysis was extended for use with potential-based TDIEs for PEC objects in [8], where it was shown how selection of correct temporal basis functions was critical to the stability of MOT discretizations of the potential-based TDIEs. In this section, we discuss how the TDIEs presented in Sections 2.2.3 can be stably discretized. Although not rigorously discussed, the selection of unknown functions to be discretized and the basis and testing schemes are heavily guided by the functional analysis methods presented in [7, 8]. In addition to selecting correct basis and testing schemes, accurate numerical integration methods must be used to achieve stable results. In particular, we utilize the method presented in [12].

3.1. Temporal Functions

To begin, we note that these equations are on a similar temporal scale to the potential-based TDIEs presented in [8]. As a result, it is concluded that $\mathbf{J}$ and Π should be appropriate unknown functions to be used. Further, the same integral operators are present so that the same temporal discretization for these unknowns will be acceptable. In particular, this uses a pulse function (constant over two time steps) as basis functions in a MOT scheme.

For simplicity, it is desirable to use other unknown functions that can be discretized with the same temporal basis function in a MOT scheme. For this to be the case, the additional unknown functions will need to have the same temporal regularity as $\mathbf{J}$ and Π. This was built into our derivation in Section 2 by writing the equations in terms of $\mathbf{m} = \hat{n}'\times\dot{\mathbf{A}}$ and $\Psi = \dot{\varphi}$. That these are correct choices can be intuitively seen in the following way. Beginning with $\mathbf{m}$, the symmetry of Maxwell's equations suggests that $\mathbf{J}$ and $\mathbf{M}$ should have the same temporal regularity, where $\mathbf{M} = -\hat{n}'\times\mathbf{E}$. Considering this, it is seen that $\mathbf{m}$ is a component of $\mathbf{M}$ and so should also utilize the same basis function as $\mathbf{J}$. In a similar manner, Ψ should be used as an unknown so that it has the same temporal regularity as the other unknown functions (e.g., $\Pi = \hat{n}'\cdot\dot{\mathbf{A}}$), which all have either a spatial or temporal derivative applied to them. More rigorous justification that φ as an unknown would require a different temporal basis function is given in [7].

3.2. Spatial Functions

Although the unknown functions and equations have been carefully selected so the same temporal basis functions can be used for all unknowns, the practical stability of these equations are not guaranteed. The further aspect that is needed is the correct selection of spatial basis and testing functions for key integral operators. In particular, both $\mathbf{J}$ and $\mathbf{m}$ need div-conforming functions, so $\mathbf{J}$ is discretized with RWGs and $\mathbf{m}$ with Buffa-Christiansen (BC) functions [13]. Note that if $\mathbf{m}$ were to use RWG functions the resulting system would be unstable due to the poorly tested identity operator for $\mathbf{m}$.

To simplify computation of far-field results, it is desirable to be able to recover $\mathbf{M}$ in post-processing. This is possible by selecting a spatial basis function for Ψ that can have the surface gradient taken of it. The classic linear nodal basis function used in finite element methods is one particular option, which also meets the spatial regularity properties needed by the integral operators that act on Ψ. [7]. To arrive at a square matrix system, Π should be discretized with a function associated with mesh nodes (similar to Ψ). One simple option that has the correct spatial regularity is a nodal pulse function, i.e., it is a constant over all triangles attached to the node the function is associated with.

In summary, the following spatial basis functions will be used for the following unknowns: RWG functions for $\mathbf{J}$, nodal pulse functions for Π, BC functions for $\mathbf{m}$, and linear nodal functions for Ψ. Spatial testing will use RWG functions for (33) and (35), and nodal pulse functions will be used to test (34) and (36).

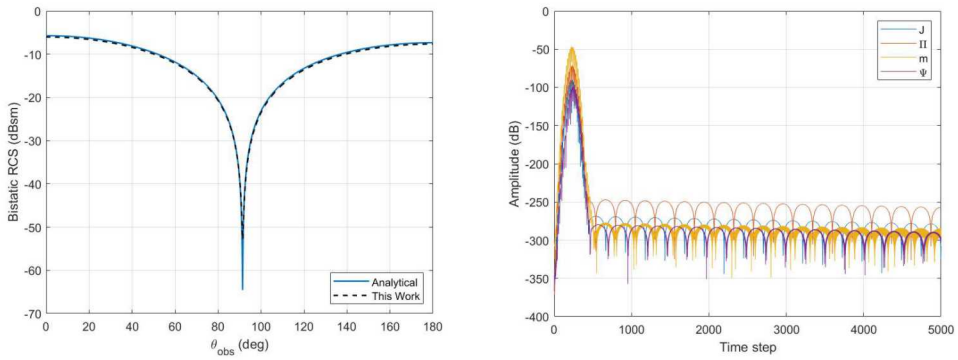

(a) (b)

Figure 2: Accuracy and stability of this formulation for scattering from a sphere: (a) RCS at 30 MHz and (b) late-time stability of sample basis function coefficients.

4. NUMERICAL RESULTS

With all the necessary details now discussed, numerical results are presented for the formulation presented in this work. Two simulations are performed to illustrate the stability of the method, with accuracy tested by comparing against an analytical solution for a dielectric sphere. We conclude the section by commenting on the lack of low frequency performance of these equations.

The first simulation considered is for a 1 meter radius sphere with a relative permittivity of 2.56. The incident vector potential is assumed to be a plane wave with a temporal profile defined by a modulated Gaussian pulse with a center frequency of 30 MHz and a bandwidth of 15 MHz. A time step of 1.11 ns was used for this simulation. Since the source is assumed to be in the far-field, the incident scalar potential is set to 0 [11]. The incoming wave propagates in the $+\hat{z}$-direction and is polarized in the $+\hat{x}$-direction. Sample results are shown in Fig. 2, where it is seen that good accuracy is achieved at the center frequency of 30 MHz, verifying the formulation. Due to the size of the overall matrix system, an eigenvalue stability analysis was not performed for this simulation. In lieu of this rigorous test, sample values of the solved for basis function coefficients are plotted as a function of time for approximately 450 transits of the geometry in Fig. 2(b).

The second simulation analyzes a more challenging geometry to demonstrate the stability of the discretization. The geometry analyzed is generated as a typical double ogive body-of-revolution that is then shrunk in one dimension by a factor of 10 to make it very thin. The generating equations are

$$\rho(x) = \begin{cases} \dfrac{5f(x)}{1-\cos(46.4^\circ)}, & \text{for } -12.5 < x < 0 \\ \dfrac{5g(x)}{1-\cos(22.62^\circ)}, & \text{for } 0 < x < 25, \end{cases} \tag{37}$$

where

$$f(x) = \sqrt{1-\left(\frac{x}{12.5}\right)^2 \sin^2(46.6^\circ)} - \cos(46.6^\circ), \tag{38}$$

$$g(x) = \sqrt{1-\left(\frac{x}{25}\right)^2 \sin^2(22.62^\circ)} - \cos(22.62^\circ), \tag{39}$$

and all dimensions are in inches. This object is shown in Fig. 3(a). The incident vector potential has a center frequency of 40 MHz and a bandwidth of 30 MHz. A time step of 0.71 ns was used for this simulation. Sample values of the solved for basis function coefficients are plotted as a function of time for approximately 500 transits of the geometry in Fig. 3(b), demonstrating the good stability properties of the discretization approach presented.

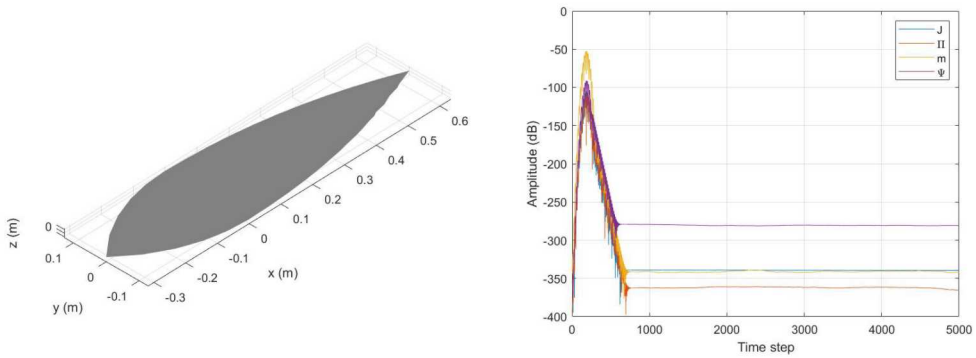

(a) (b)

Figure 3: Stability of the discretization for a more challenging thin and complicated geometry: (a) geometry analyzed and (b) late-time stability of sample basis function coefficients.

Unfortunately, this combination of equations loses accuracy as the frequency is lowered until the simulation becomes unusable due to inaccuracies. Despite this loss of accuracy, the simulations have not become numerically unstable even for a simulation of a 1 meter radius sphere with a 1 Hz center frequency. It is anticipated that supplementing these equations by enforcing additional integral equations corresponding to more boundary conditions will improve the low frequency performance. This will be investigated in our future work.

5. CONCLUSION

This work presented the systematic development of potential-based TDIEs applicable to dielectric regions. The foundation of this is the development of coupled integral representations of the solutions to the scalar and vector potential wave equations in the time domain. The derivation of these integral representations were performed to specifically arrive at a form that can be easily used to develop stable TDIEs when using a MOT discretization approach. Correspondingly, guidelines for selecting appropriate basis and testing functions to achieve stable numerical results based on the Sobolev space mapping properties of these time domain integral operators were presented. Numerical results were presented which validated the accuracy and stability properties of our formulation and discretization approach. Our future work will address the issues of the low frequency inaccuracy of these equations so they may be used in analyzing applications of interest.

ACKNOWLEDGMENT

This work was supported by AF Sub RRI PO0539, NSF ECCS 169195, and the Distinguished Professorship Grant at Purdue University.

This paper describes objective technical results and analysis. Any subjective views or opinions that might be expressed in the paper do not necessarily represent the views of the U.S. Department of Energy or the United States Government.

Sandia National Laboratories is a multimission laboratory managed and operated by National Technology & Engineering Solutions of Sandia, LLC, a wholly owned subsidiary of Honeywell International Inc., for the U.S. Department of Energy's National Nuclear Security Administration under contract DE-NA0003525.

REFERENCES

1. Y. P. Chen, W. E. I. Sha, W. C. H. Choy, L. Jiang, and W. C. Chew, "Study on spontaneous emission in complex multilayered plasmonic system via surface integral equation approach with layered medium Greens function," *Optics Express*, vol. 20, no. 18, pp. 20 210–20 221, 2012.
2. A. Y. Liu and W. C. Chew, "Dressed atom fields and dressed states in waveguide quantum electrodynamics," *IEEE Journal on Multiscale and Multiphysics Computational Techniques*, vol. 2, pp. 58–65, 2017.
3. J. L. Xiong, M. S. Tong, P. Atkins, and W. C. Chew, "Efficient evaluation of Casimir force in arbitrary three-dimensional geometries by integral equation methods," *Physics Letters A*, vol. 374, no. 25, pp. 2517–2520, 2010.

4. A. W. Rodriguez, A. P. McCauley, J. D. Joannopoulos, and S. G. Johnson, "Casimir forces in the time domain: Theory," *Physical Review A*, vol. 80, no. 1, p. 012115, 2009.
5. W. C. Chew, "Vector potential electromagnetics with generalized gauge for inhomogeneous media: Formulation," *Progress In Electromagnetics Research*, vol. 149, pp. 69–84, 2014.
6. T. E. Roth and W. C. Chew, "Development of stable A-Φ time-domain integral equations for multiscale electromagnetics," *IEEE Journal on Multiscale and Multiphysics Computational Techniques*, vol. 3, pp. 255–265, 2018.
7. T. Ha-Duong, "On retarded potential boundary integral equations and their discretisation," in *Topics in Computational Wave Propagation*. Springer, 2003, pp. 301–336.
8. T. E. Roth and W. C. Chew, "Stability analysis of A-Φ time domain integral equations for multiscale electromagnetics," under review, 2019.
9. W. C. Chew, *Waves and Fields in Inhomogeneous Media*. IEEE Press, 1995.
10. J. A. Stratton, *Electromagnetic Theory*. John Wiley & Sons, 2007.
11. Q. S. Liu, S. Sun, and W. C. Chew, "A potential based integral equation method for low-frequency electromagnetic problems," *IEEE Transactions on Antennas and Propagation*, vol. 66, no. 3, pp. 1413–1426, 2018.
12. A. J. Pray, N. V. Nair, and B. Shanker, "Stability properties of the time domain electric field integral equation using a separable approximation for the convolution with the retarded potential," *IEEE Transactions on Antennas and Propagation*, vol. 60, no. 8, pp. 3772–3781, 2012.
13. K. Cools, F. Andriulli, D. De Zutter, and E. Michielssen, "Accurate and conforming mixed discretization of the MFIE," *IEEE Antennas and Wireless Propagation Letters*, vol. 10, pp. 528–531, 2011.